

Dmitry V. Guzatov, Sergey V. Gaponenko* and Hilmi V. Demir

Colloidal Photoluminescent Refractive Index Nanosensor Using Plasmonic Effects

<https://doi.org/10.1515/zpch-2018-1127>

Received January 28, 2018; accepted February 23, 2018

Abstract: Fluorescence enhancement by metal nanostructures which is sensitive to refractive index n of an ambient medium is suggested as an operation principle of a novel refractive index sensor for liquids. Calculations are made for spherical and spheroidal Ag particles, and potential feasibility of sensitivity of the order of $\Delta n = 10^{-4}$ is demonstrated. Sensors of this type can be made fully colloidal with metal bodies deposited on a substrate or comprising a metal layer covering colloidal assembly of dielectric particles to serve as a test strip as well as placed on a fiber tip end to get local probing of refractive index in the tip-enhanced refractometry mode. Colloidal core-shell semiconductor nanocrystals may become the best candidates for this type of sensors whereas molecular probes may be affected by chemical properties of tested liquids.

Keywords: colloidal nanostructures; fluorescence; plasmonics; refractive index; sensors.

1 Introduction

There is a practical need for affordable and cheap set-up and a procedure for monitoring of small refractive index (RI), n , change in bioliquids for medical application. In certain production processes monitoring of refractive index for liquids is also important. The extreme detection limit for small refractive index measurement as low as 10^{-7} has been reported though the technique is based on the very accurate measurements of interference patterns in a light diffrac-

*Corresponding author: **Sergey V. Gaponenko**, B. I. Stepanov Institute of Physics, National Academy of Sciences, Minsk 220072, Belarus, e-mail: s.gaponenko@ifanbel.bas-net.by

Dmitry V. Guzatov: Yanka Kupala State University of Grodno, Grodno 230023, Belarus

Hilmi V. Demir: Department of Electrical and Electronics Engineering, Department of Physics, and UNAM–Institute of Materials Science and Nanotechnology, Bilkent University, Ankara 06800, Turkey; and LUMINOUS! Center of Excellence for Semiconductor Lighting and Displays, School of Electrical and Electronic Engineering, School of Physical and Mathematical Sciences, Nanyang Technological University, 50 Nanyang Ave 639798, Singapore, Singapore

tion set-up [1]. Less sensitive but cheap and affordable approaches are also on demand. Last decades plasmonic effects have been extensively explored for refractive index sensing. The underlying mechanism in this approach is sensitivity of the extinction spectrum of metal nanospecies (nanotextured surface or nanoparticles) to the dielectric permittivity (ε) of the ambient or interfacing medium, for a non-absorbing medium $\varepsilon = n^2$ holds. Thus plasmonics offers an option to trace ambient refractive index by means of extinction spectrum measurements [2, 3]. The representative list of activity in this field can be found in Refs. [4–12]. Spherical metal nanoparticles, nanorods, nanoshells (dielectric solid spheres covered with a metal shell) and other nanoparticles with the complex shape (e.g. stars) with size 50...100 nm were found to feature the pronounced sensitivity to an ambient refractive index. The figure of merit is the extinction peak shift $\Delta\lambda$ in nm per refractive index unit (RIU). For example, the peak shift of 10 nm for RI changing from 1.4 to 1.5 gives $\Delta\lambda = 100$ nm/RIU. The simplest case of solid spheres offers approximately 250 nm/RIU for Ag nanospheres. For core-shell structures with dielectric core and metal shells (“nanoshells”) for the same dielectric core diameter a thinner metal shell offers higher sensitivity to n variation. The highest sensitivity of refractive index sensing based on the extinction peak wavelength measurements was probably reported for Au “nanorice” and measures about 800 nm/RIU [4]. For 200 nm silica core with 20 nm gold nanoshells, Tam et al. [7] reported experimental observation of more than 500 nm/RIU. Au-based nanoparticles feature less sensitive response. Au solid spheres exhibit 50–90 nm/RIU and Au nanorods show about 300 nm/RIU [12]. Keeping in mind that extinction bands are rather wide, the typical accuracy in peak position measurements without using special and expensive spectral instruments may be about 1 nm for the extinction band halfwidth (the full width at half maximum) being about 50 nm. Thus the reasonable affordable detection limit appears in the range of $\Delta n = 10^{-2}$ – 10^{-3} . Since there is a serious gap between this approach and the current limit of detection ($\Delta n = 10^{-7}$), it is reasonable to consider possible extension of the plasmonic approach to get further enhancement in sensitivity. In this paper, we suggest plasmonically enhanced photoluminescence intensity as the refraction sensitive process to develop yet another type of the plasmonic sensors.

2 The sensing principle and the model

Plasmonic enhancement of fluorescence results from the local incident field enhancement and modification of quantum yield [2, 13, 14], both processes being

sensitive to overlap of the extinction spectrum with the absorption and emission spectra of fluorescent probes [15]. Thus fluorescence intensity featuring a complicated dependence on extinction may appear to be more sensitive to the ambient refractive index than the extinction itself.

We use the well established approach to model fluorescence of a probe dipole (a molecule, a quantum dot, or an atom) located near a metal nanobody (a sphere or a spheroid) as is sketched in Figure 1. The calculation scheme and the relevant equation can be found in Ref. [14, 16]. There are three basic processes affecting luminescence intensity. First, incident local field \mathbf{E} enhancement depending on the specific point, \mathbf{r} , the incident field wavelength λ and polarization, the metal type, the body shape and dimensions. The incident field enhancement well correlates with the extinction spectrum and changes with refractive index following the extinction changes. Second, radiative decay rate enhancement occurs which depends on an emitter position \mathbf{r} , its dipole moment \mathbf{d}_0 orientation, emission wavelength λ_{em} , and generally correlates with the extinction spectrum, i.e. it depends on the metal type and the body size and shape. Third, nonradiative decay rate also experiences enhancement in the presence of the nanobody depending on the distance to metal surface and correlating rather with the dielectric function than with the extinction, i.e. non-radiative decay does not follow directly extinction shift with size and shape.

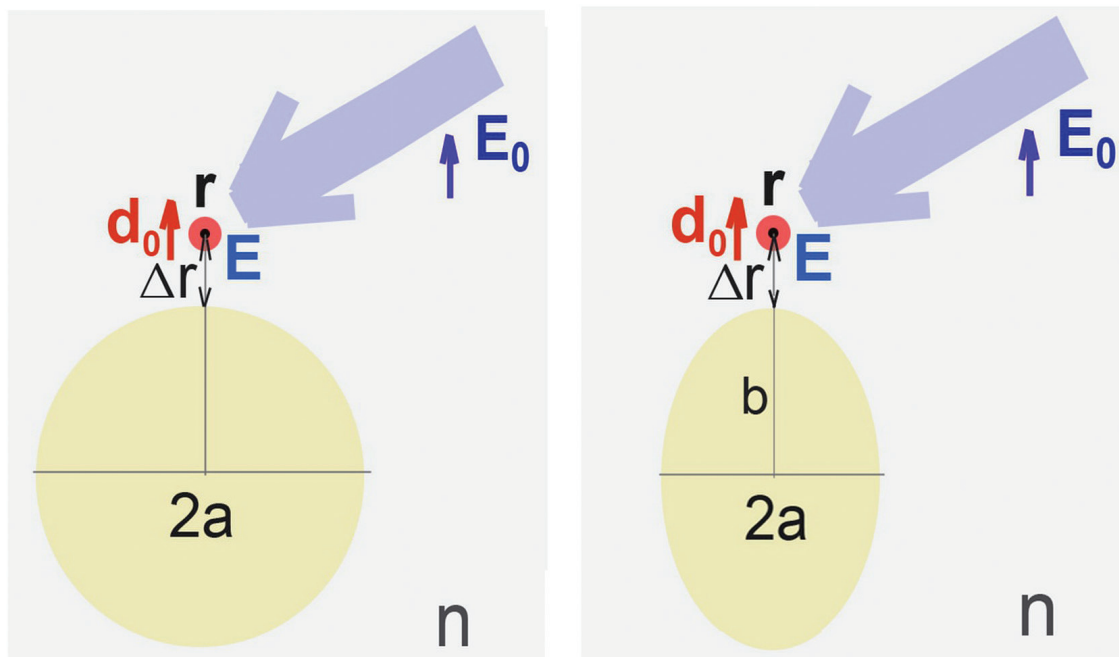


Fig. 1: Displacement of an emitter and a nanobody used in calculations. Arrows indicate orientation of an emitter dipole moment \mathbf{d}_0 and the incident radiation polarization, Δr is the distance between the metal nanobody surface and the emitter. See text for more detail.

The fluorescence enhancement factor develops as the product of local incident intensity enhancement (proportional to \mathbf{E}^2) and the quantum yield defined by the radiative and nonradiative decay rates. For perfect emitters with the intrinsic quantum yield $Q_0 = 1$, a metal body will necessarily promote quenching with $Q(\mathbf{r}) < Q_0$. However, for emitters with low $Q_0 < 1$, quenching may not be pronounced and even $Q(\mathbf{r}) > Q_0$ can be obtained [16]. Generally, in simple colloidal metal structures with a few nm dielectric spacers (oxide shells, polyelectrolytes, Langmuir – Blodgett films) perfect emitters show enhancement up to 10 times whereas poor emitters show enhancement factors rising inversely proportional to Q_0 , i.e. 100 times enhancement becomes feasible for $Q_0 < 0.1$. Special arrangements of nanobodies, nanoantennas, and periodic structures enable higher enhancement provided an emitter is placed in the proper positions.

We shall consider here the metal spheres and spheroids which are appreciated in many works since these allow analytical calculations, with full account of size effect in scattering for spheres (Mie theory) and using the quasistatic model for spheroids (implying a nanobody is much smaller than λ). Spheroids are supposed to represent a reasonable approximation for nanorods [17]. Both types of particles can be obtained by means of colloidal chemistry without lithography, epitaxy and etching thus enabling chip and versatile bottom-up engineering meeting the general concept of colloidal photonics as an emerging technology platform [18]. The most favorable situations for fluorescence enhancement are shown in Figure 1. Since very large number of the above listed parameters is involved we shall fix most of them using the realistic and reasonable values and cases to illustrate the essence of the sensing conception.

The photoluminescence intensity enhancement factor F_{PL} for a dipole emitter near a metal nanobody at point \mathbf{r} can be calculated as a product of the incident excitation intensity enhancement G and emitter quantum yield modification Q/Q_0 , where Q_0 is the intrinsic quantum yield in vacuum,

$$F_{PL}(\mathbf{r}, \omega, \omega') = G(\mathbf{r}, \omega) \frac{Q(\mathbf{r}, \omega')}{Q_0(\omega')} \quad (1)$$

$$= \frac{|\mathbf{E}(\mathbf{r}, \omega)|^2}{|\mathbf{E}_0(\mathbf{r}, \omega)|^2} \left(\frac{\gamma_{\text{rad}}(\mathbf{r}, \omega')/\gamma_0(\omega')}{Q_0(\omega')[\gamma_{\text{rad}}(\mathbf{r}, \omega')/\gamma_0(\omega') + \gamma_{\text{nonrad}}(\mathbf{r}, \omega')/\gamma_0(\omega') - 1] + 1} \right).$$

Here \mathbf{E} (\mathbf{E}_0) is electric field at the point of interest with (without) a metal body; ω (ω') is the excitation (emission) frequency; γ_{rad} (γ_{nonrad}) is radiative (nonradiative) decay rate of the emitter at the point of interest in presence of a metal nanobody; γ_0 is its decay rate in vacuum; $Q_0 = \gamma_0/(\gamma_0 + \gamma_{\text{int}})$ is the intrinsic quantum yield of the

emitter with γ_{int} being the intrinsic nonradiative decay rate (it does not depend on the nanobody). We consider that polarization of the incident radiation and the dipole moment orientation coincide which enables the maximal photoluminescence enhancement. The enhancement factor depends on the distance between the metal nanobody surface and the emitter, $\Delta\mathbf{r}$. More detail on the calculation scheme and explicit equations for the parameters involved can be retrieved in Refs. [14, 16].

3 Results and discussion

3.1 Nanospheres

Figure 2 shows a set of the extinction spectra for Ag spheres to recall the primary shift of extinction spectra with familiar 200 nm/RIU sensitivity. The extinction spectrum also defines the spectral range where the expected fluorescence enhancement will occur. Ambient refractive index growth moves the extinction spectrum and the radiative decay rate enhancement spectrum to longer wavelength and thus photoluminescence will be higher enhanced if originally extinction peak was in the short-wave range as compared to photoluminescence excitation and emission spectra. This approach is illustrated in Figure 3 where the photoluminescence enhancement factor F_{PL} versus the ambient refractive

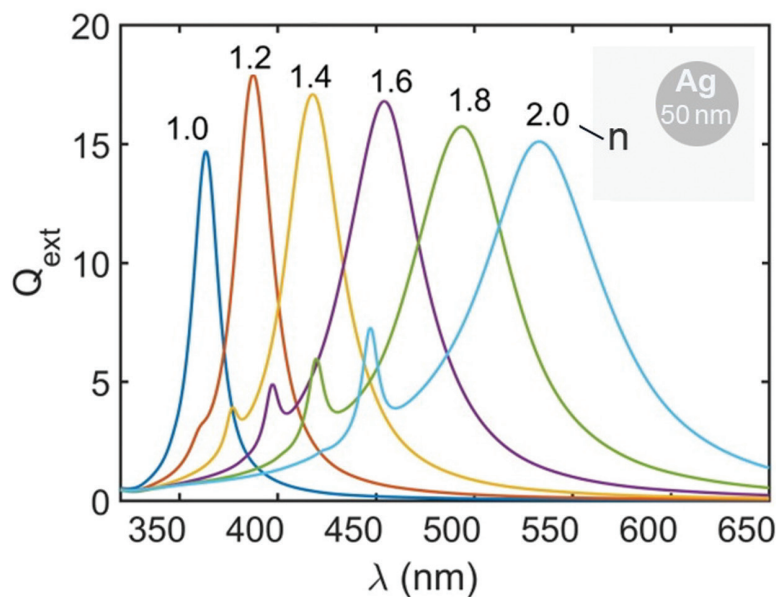


Fig. 2: Calculated dimensionless extinction spectra of silver spherical nanoparticles with 50 nm diameter embedded in a medium with refractive index ranging from 1 to 2.

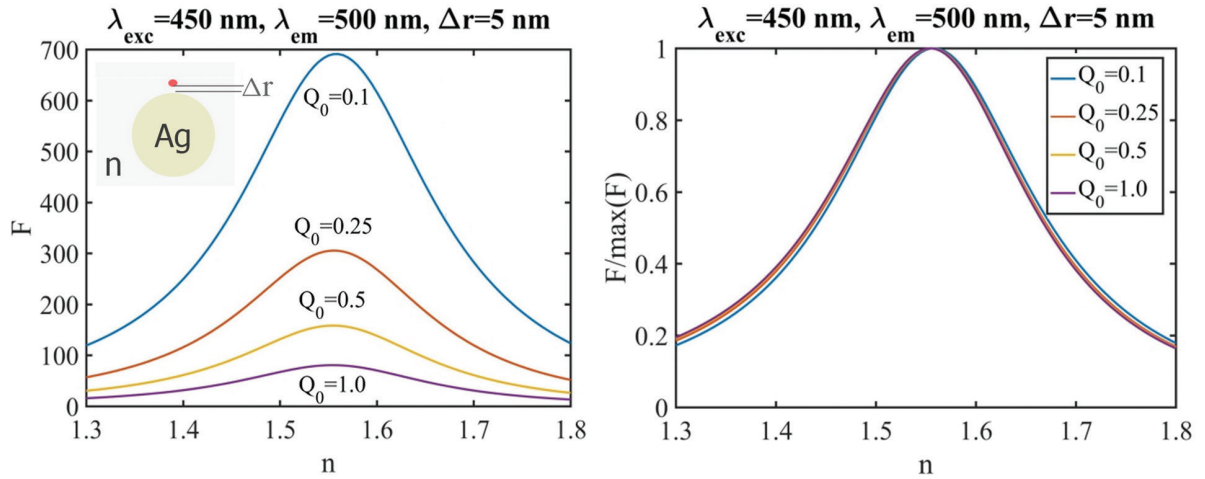


Fig. 3: Photoluminescence enhancement factors versus refractive index of the ambient medium for the case of silver spherical nanoparticles (50 nm diameter) for various intrinsic quantum yield of the emitter Q_0 with emission wavelength 500 nm and excitation wavelength 450 nm. (Left) absolute enhancement factors; (Right) normalized enhancement factors.

index is plotted for Ag spheres for various quantum yields in the absolute and in the normalized units. Here the figure of merit (FOM) is the refraction-dependent relative change in fluorescence intensity which is proportional to the relative change in the fluorescence enhancement factor F_{PL} ,

$$\text{FOM} = \frac{\Delta I / I}{\Delta n} = \frac{\Delta F_{PL} / F_{PL}}{\Delta n}. \quad (2)$$

Both positive and negative slopes in the $F_{PL}(n)$ function can be used, i.e. for example, that the refractive index growth may give rise either to growth or to drop in photoluminescence intensity depending on the set of parameters chosen for an experimental implementation. One can see that the sensitivity is feasible about 1000%/RIU for n close to 1.45 (positive slope) and 1.65 (negative slope). Implying 1% sensitivity in intensity measurements, one can arrive at the limit of detection (LOD) close to 0.001 RIU. Noteworthy, when comparing with the extinction peak based approach, monitoring of intensity may appear to be performed with cheaper equipment than monitoring spectrum shape to evaluate its peak. Figure 3 (right panel) shows that sensitivity to refractive index does not actually depend on the absolute enhancement factors and on the intrinsic quantum yield. Though enhancement is higher for the lower quantum yield, its relative sensitivity to the refraction change remains the same. One should bear in mind that FOM changes across the n -axis so that for the target n range with the fixed emission and excitation wavelengths the optimal sphere diameter exists.

3.2 Nanorods

For spheroids extinction spectra and photoluminescence enhancement are rather narrow as compared to spheres and depend on both length and aspect ratio. Since the spectral range of photoluminescence enhancement correlates with the spectral position of the extinction band defined by the morphological resonance, we first evaluate the dependence of this band versus refractive index for various aspect ratio of a silver spheroid. In Figure 4 the peak extinction is presented for various aspect ratio a/b values in the range of refractive index from 1 to 1.5 for the length $2b$ equal to 20 and 40 nm, and 450 nm wavelength (in a vacuum), respectively. The nanobody-emitter alignment corresponds to Figure 1 (right).

Results in Figure 4 indicate that for the parameters (the wavelength and the refractive index range) the most efficient enhancement occurs for the aspect ratio 0.4...0.7. Figure 5 shows the photoluminescence enhancement factor dependencies in detail for the emission wavelength 500 nm and excitation wavelength 450 nm. For every given aspect ratio enhancement change with refractive index is dependent on the refractive index value but the maximal sensitivity (the slope of the $F_{PL}(n)$ function) remains approximately the same. Thus a reasonable recipe will be to adjust aspect ratio (or possibly excitation and emission wavelengths) for the desirable n range. The figure of merit can reach 10⁴⁰%/RIU which means that limit of detection will be down to $\Delta n = 10^{-4}$ RIU supposing 1% photoluminescence intensity detectivity.

The maximal achievable slope of the $F_{PL}(n)$ function seems to be not very much sensitive to the spheroid length and the emitter-metal spacing Δr . However, in practical devices higher PL intensities may be appreciated to make detection easier in terms of signal-to-noise ratio, data acquisition time or detector grade.

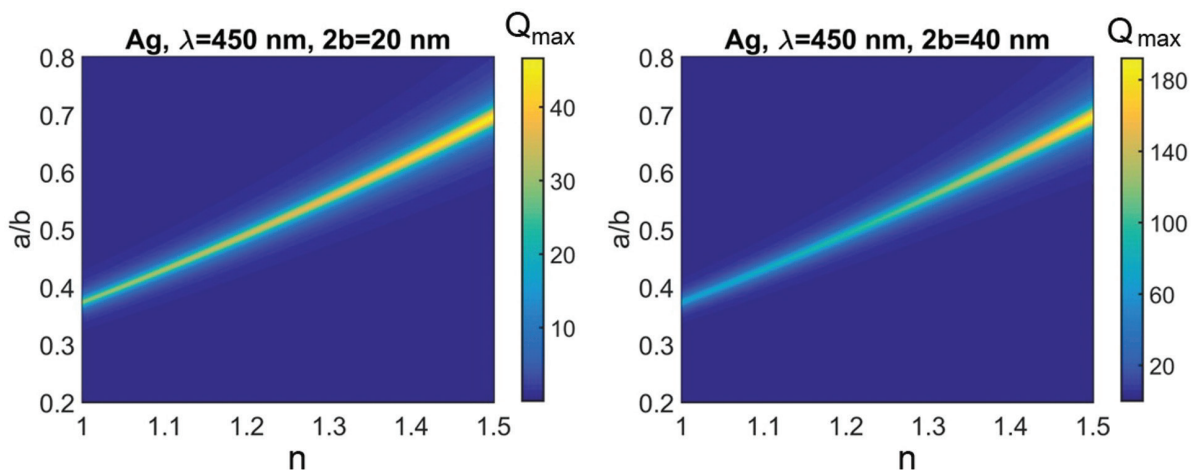


Fig. 4: Calculated maximal dimensionless extinction of silver nanorods at the selected excitation wavelength 450 nm versus ambient medium refractive index n and aspect ratio a/b .

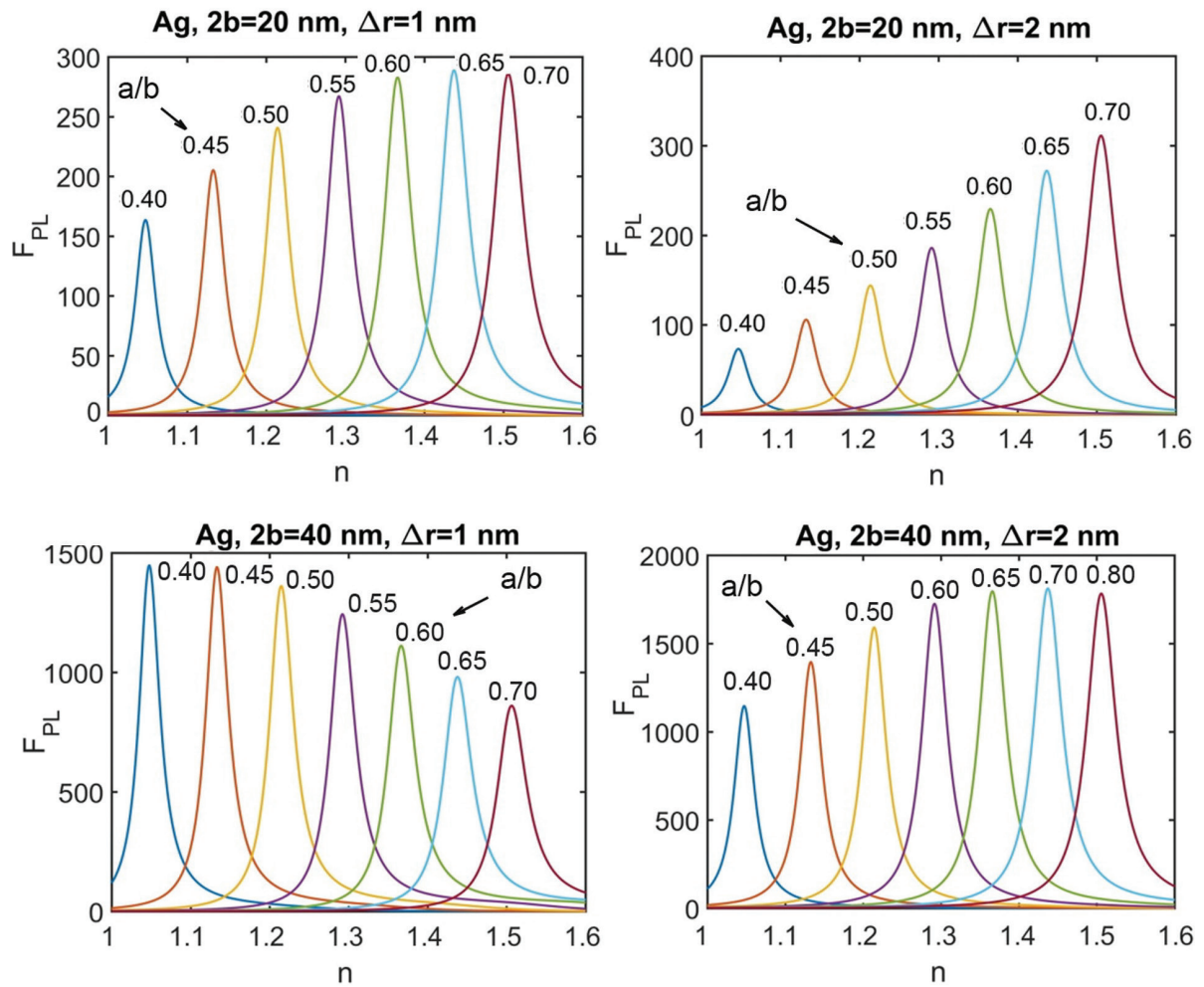


Fig. 5: Calculated photoluminescence enhancement factor for various aspect ratio for a silver spheroid. Emission and excitation wavelengths are 500 and 450 nm (in vacuum), respectively. Spheroid length $2b = 20$ nm (top) and 40 nm (bottom); an emitter metal spacing $\Delta r = 1$ nm (left) and 2 nm (right).

Therefore in Figure 6 we show sample calculations for $F_{PL}(\Delta r)$ for the two selected cases where the maximal F_{PL} is reached at $\Delta r = 1$ nm for the spheroid length 20 nm and $\Delta r = 2$ nm for the spheroid length 40 nm.

3.3 Application issues

The results of calculations present the ideal cases under an assumption that the refractive index is the only ambient parameter affecting photoluminescence intensity. In this context, possible effects of other parameters should be taken into account and are briefly discussed here.

First, change in refractive index when being caused by the chemical content may affect photoluminescence intensity and spectrum because of

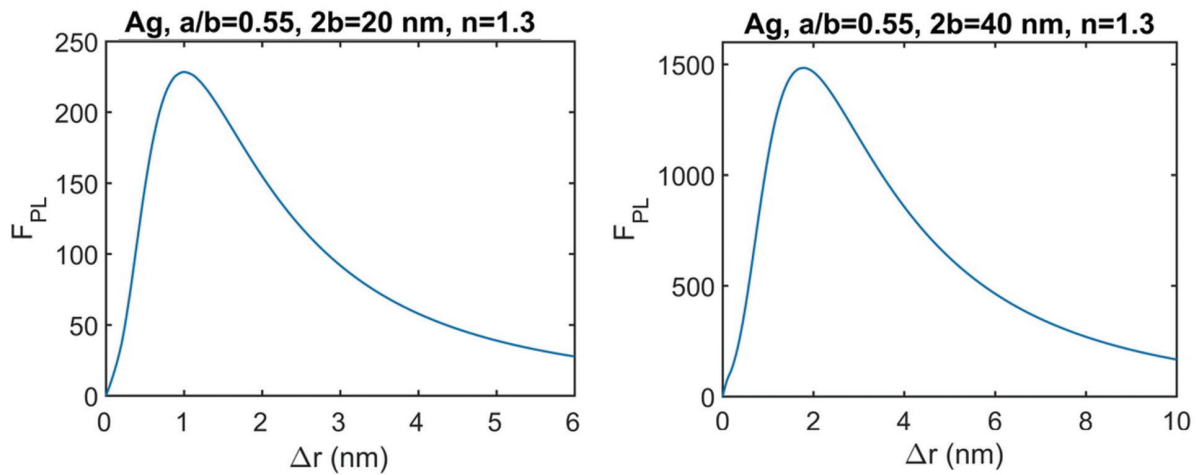


Fig. 6: Photoluminescence intensity enhancement factor versus emitter – metal spacing for the two values of the spheroid length (20 nm and 40 nm) and refractive index $n=1.3$. The emission wavelength is 500 nm, the excitation wavelength is 450 nm.

chemical effects, pH value and polarity. In this case, molecular fluorophores may appear to be not the best emitters for the proposed sensor applications. For every specific case of analysis, robustness of a given molecular probe should be checked. In this context, colloidal quantum dots, and especially core-shell quantum dot emitters with thick shells [19–21] may appear more robust and durable. Lanthanides or transition metal ions in nanocrystals [22, 23] may also become the advantageous probes. Refraction sensitive luminescent tips can be fabricated by means of colloidal crystals covered with noble metals [24] as well as by any other technique enabling cheap fabrication of nanostructured metal surface [25–27] with subsequent linkage of fluorescent probes via a dielectric spacer [28].

Second, an emitter – nanobody alignment presented in Figure 1 corresponds to the maximal enhancement of the photoluminescence intensity. In real situations, random orientation of emitters and size dispersion in an ensemble of metal nanospheres will make enhancement somewhat lower [14], and the FOM value can be affected as well. However, owing to the symmetry of the problem the specific position of an emitter versus metal sphere will have no effect provided that the emitter – metal distance is controlled (via spacer thickness). The situation is more complicated for the case of nanorods (spheroids) because for these nanobodies not only emitter orientation and distance to metal but also the specific position of an emitter is important. Therefore in the real situations the FOM numbers calculated may not be achieved and should be treated as reference values corresponding to the ideal and controllable alignment.

It is clear that colloidal nanoparticles can be adsorbed on glass or polymer substrates which can then serve as test strips. Fluorescent probes with nanoparticles

can be attached at the end of an optical fiber, and then local probing of refractive index can be performed using a fiber to guide both incident and emitted radiation. This “tip-enhanced refractometry” mode is most easy to be performed with fluorescence based plasmonic sensors rather than with extinction based ones.

4 Conclusions

A novel type of the refractive index sensor is proposed based on fluorescence intensity dependence in plasmonic nanostructures upon an ambient medium refractive index n value. The figure of merit (FOM) for this type of sensor is the relative photoluminescence intensity change per refractive index unit. For silver nanostructures in the range of typical liquids ($n = 1.3 \dots 1.5$) our calculations show $FOM = 10^3\%/RIU$ for spheres and $10^4\%/RIU$ for spheroids which enable limit of detection of $\Delta n = 10^{-3}$ and 10^{-4} supposing the intensity detection accuracy of 1%. These numbers correspond to the ideal cases of emitter – metal alignment and can be lower in real experiments. Core-shell colloidal quantum dots look promising probes for this type of refractometry. Local probing of refractive index changes in the tip-enhanced refractometry mode can be readily performed using a fiber for both excitation and detection of photoluminescence.

Acknowledgement: The work has been supported by BRFFR-TUBITAK #F16T/A-010 and TUBITAK no.115E679, and in part by Singapore National Research Foundation under NRF-NRFI2016-08.

References

1. D. Markov, D. Begari, D. J. Bornhop, *Anal. Chem.* **4** (2002) 5438.
2. S. V. Gaponenko, *Introduction to Nanophotonics*, Cambridge University Press, Cambridge UK (2010).
3. N. Jiang, X. Zhuo, J. Wang, *Chem. Rev.* (2017). DOI: 10.1021/acs.chemrev.7b00252
4. K. M. Mayer, J. Y. Hafner, *Chem. Rev.* **111** (2011) 3828.
5. K. A. Willets, R. P. Van Duyne, *Annu. Rev. Phys. Chem.* **58** (2007) 267.
6. Y. Sun, Y. Xia, *Anal. Chem.* **74** (2002) 5297.
7. F. Tam, C. Moran, N. Halas, *J. Phys. Chem. B* **108** (2004) 17290.
8. M. M. Miller, A. A. Lazarides, *J. Phys. Chem. B* **109** (2005) 21556.
9. H. Liao, C. L. Nehl, J. H. Hafner, *Nanomedicine* **1** (2006) 201.
10. J. Zhu, F. Zhang, J. Li, J. Zhao, *Sens. Actuators, B: Chem.* **183** (2013) 143.
11. P. K. Jain, M. A. El-Sayed, *J. Phys. Chem. C* **111** (2007) 17451.
12. H. Chen, X. S. Kou, Z. Yang, W. H. Ni, J. F. Wang, *Langmuir* **24** (2008) 5233.

13. C. D. Geddes (Ed.), *Metal-Enhanced Fluorescence*, John Wiley & Sons, Hoboken, New Jersey (2010).
14. D. V. Guzatov, S. V. Vaschenko, V. V. Stankevich, A. Ya. Lunevich, Y. F. Glukhov, S. V. Gaponenko, *J. Phys. Chem. C* **116** (2012) 10723.
15. Y. Chen, K. Munechika, D. S. Ginger, *Nano Lett.* **7** (2007) 690.
16. D. V. Guzatov, S. V. Gaponenko, H. V. Demir, *AIP Adv.* **8**, (2018) 015324.
17. H. Chen, L. Shao, Q. Li, J. Wang, *Chem. Soc. Rev.* **42** (2013) 2679.
18. S. Gaponenko, H. V. Demir, C. Seassal, U. Woggon, *Opt. Express* **24** (2016) A430.
19. A. Eychmüller, *J. Phys. Chem. B* **104** (2000) 6514.
20. A. Eychmüller, A. L. Rogach, *Pure Appl. Chem.* **72** (2000) 179.
21. N. Gaponik, S. G. Hickey, D. Dorfs, A. L. Rogach, A. Eychmüller, *Small* **6** (2010) 1364.
22. J. T. Van Wijngaarden, M. M. Van Schooneveld, C. de Mello Donegá, A. Meijerink, *Europhys. Lett.* **93** (2011) 57005.
23. M. V. Artemyev, L. I. Gurinovich, A. P. Stupak, S. V. Gaponenko, *Phys. Stat. Sol. (b)* **224** (2001) 191.
24. S. V. Gaponenko, A. A. Gaiduk, O. S. Kulakovich, S. A. Maskevich, N. D. Strekal, O. A. Prokhorov, V. M. Shelekhina, *J. Exper. Theor. Phys. Lett.* **74** (2001) 309.
25. C. Zhu, D. Du, A. Eychmüller, Y. Lin, *Chem. Rev.* **115** (2015) 8896.
26. L. Lu, I. Randjelovic, R. Capek, N. Gaponik, J. Yang, H. Zhang, A. Eychmüller, *Chem. Mater.* **17** (2005) 5731.
27. V. Lesnyak, A. Wolf, A. Dubavik, L. Borchardt, S. V. Voitekhovich, N. Gaponik, S. Kaskel, A. Eychmüller, *J. Amer. Chem. Soc.* **133** (2011) 13413.
28. S. V. Vaschenko, A. A. Ramanenka, D. V. Guzatov, V. V. Stankevich, A. Y. Lunevich, Y. F. Glukhov, I. F. Sveklo, S. V. Gaponenko, *J. Nanophotonics* **6** (2012) 061710.